

# Macroscale Modeling of Geochemistry Influence on Polymer and Low-Salinity Waterflooding in Carbonate Oil Reservoirs

Angelo Kennedy Lino Limaluka, Yogarajah Elakneswaran,\* and Naoki Hiroyoshi

Cite This: *ACS Omega* 2024, 9, 17174–17184

Read Online

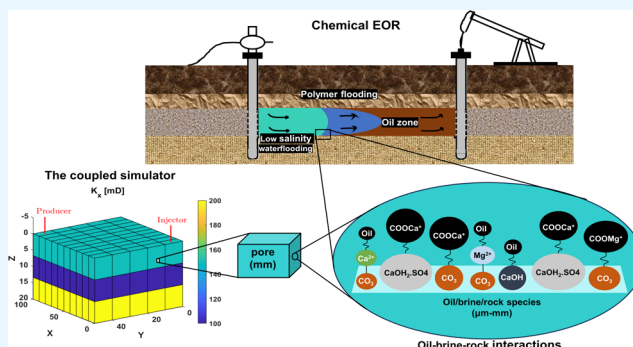
ACCESS |

Metrics &amp; More

Article Recommendations

Supporting Information

**ABSTRACT:** The enhancement of oil recovery (EOR) through low-salinity waterflooding (LSWF) and the emerging hybrid with a polymer (LSP) has proven to be effective at macroscale investigations and cost-effective with ease of operation at field-scale tests. Their application in carbonate oil reservoirs, which typically occur oil-wet, presents a particularly essential capacity given that over half of the global oil reserves are hosted in carbonate formation. However, modeling the mechanisms involved to predict and evaluate the performance of low salinity-based EOR at a large scale is complex and requires the integration of geochemistry in reservoir simulation to upscale the interfacial interactions of crude oil, brine, and rock observed at the micrometer scale. This study presents an integrated approach that combines MRST's polymer model with PHREEQC geochemical modeling to simulate LSWF at the reservoir scale. Using single-phase and multiphase experimental flooding data for validation, the coupled model was shown to accurately predict effluent ionic and oil recovery profiles. The simulation of LSWF and LSP both exhibited additional tertiary oil recovery, with LSWF and LSP showing 3 and 2%, respectively, which are consistent with previously reported field and core flooding results. Furthermore, the sequential application of formation water (FW), LSWF, and LSP flooding in secondary mode showed a high increase in oil recovery, with oil recovery percentages of 61, 20, and 19%, respectively. However, the FW results were 50% lower compared to regular core flooding due to upscaling limitations. The modeling of vertical and anisotropic permeability heterogeneity effects showed a positive synergy with low-salinity floodings, resulting in a 4% drop and 3 and 1% increase in FW, LSWF, and LSP, respectively. These findings demonstrate the potential of the coupled MRST-PHREEQC model in accurately simulating hydrogeochemical interactions during LSWF/LSP at the reservoir scale, providing valuable insights for the optimization of low salinity-based EOR strategies in carbonate reservoirs.



## 1. INTRODUCTION

Presently, oil remains a major source of the global energy, accounting for at least a third of the total consumption.<sup>1</sup> Recent data from the first quarter of 2023 indicate a record-breaking global oil demand of 102.2 million barrels per day (mb/d), driven by the economic growth in China and the United States, high oil prices, and increasing demand in non-OECD countries.<sup>2</sup> The International Energy Agency (IEA) forecasts this demand to remain high throughout the next decade, peaking at around 103 mb/day in the mid-2030s. However, the availability of easily accessible oil reserves is diminishing, posing challenges to meeting this growing demand. Furthermore, the average conventional oil recovery factor achieved through primary and secondary methods remains below 30% on a global scale.<sup>3</sup> As a result, the need for improved and enhanced oil recovery (IOR/EOR) processes has become more important, particularly given that at least 60% of the crude oil reserves are heavy oil carbonate formations.<sup>4</sup>

In the previous decade, data showed that approximately 4% (4 mb/d) of the world's daily oil consumption was produced through EOR.<sup>5</sup> Most of this came from thermal EOR (around 3 mb/d) and miscible gas EOR (approximately 0.4 mb/d);<sup>5</sup> notable successful implementation of thermal EOR methods has been in heavy oilfields such as in Alberta (Canada), Bakersfield (California), Daqing (China), and the Orinoco Belt (Venezuela). Also, CO<sub>2</sub>-EOR has notably been implemented in the Permian Basin (US) and Weyburn (Canada), while chemical EOR (cEOR) techniques have predominantly been applied in China's oilfields, such as Shengli and Daqing. According to data from 2008, the global production through

Received: December 14, 2023

Revised: February 6, 2024

Accepted: February 9, 2024

Published: April 5, 2024



cEOR and miscible gas was in the same range of about one-third mb/d.<sup>5</sup> However, since 2021, there has been an increase in large-scale field applications of cEOR using polymer flooding, with projects being conducted in various countries, including Canada, Argentina, and India.<sup>6</sup>

Other forms of cEOR have also shown growth over the past decade, except for surfactant and surfactant-hybrid flooding, which face challenges in reservoir conditions characterized by high salinity and temperature.<sup>2,5</sup> Moreover, implementing EOR/cEOR techniques can be expensive, involving capital expenditures for materials, equipment, chemicals, well modifications, monitoring, and operations.<sup>5,6</sup> These methods are typically economically viable when oil prices range from USD 20 to 80 per barrel, such as in the current period. However, certain water-based oil recovery techniques, such as low-salinity waterflooding (LSWF), have been developed and applied with limited facility retrofitting and low costs. Additionally, hybrid EOR approaches, such as low-salinity polymer flooding (LSP), have shown promise due to their synergistic properties.

LSWF is a secondary and tertiary oil production technique that involves injecting diluted formation water, seawater, or smart water to enhance the oil recovery process.<sup>7,8</sup> Despite its cost-effectiveness, environmental benefits, and potential for up to 15% additional oil recovery, LSWF has not gained widespread operational acceptance and remains largely confined to experimental applications.<sup>9</sup> The main challenge lies in upscaling the results of LSWF mechanisms studied across various reservoir scales to generate standardized operational parameters, reduce associated reservoir damage risks, and facilitate broader LSWF field implementation.<sup>4,10–12</sup> The commercialization and maturity of LSWF have been hindered by these challenges, but extensive microscale studies have revealed that wettability alteration plays a crucial role in LSWF interactions. As a result, modeling wettability alteration has become the primary focus when simulating LSWF in both core and large-scale models across different platforms.<sup>13–16</sup>

Popular industry reservoir simulators such as UTCHEM (University of Texas Chemical Flooding Simulator) and Schlumberger's ECLIPSE have been utilized to model LSWF, along with other newer platforms such as SINTEF's MATLAB Reservoir Simulator Toolbox (MRST). For instance, in UTCHEM, Korrani et al.<sup>17</sup> employed PHREEQC to model LSWF geochemistry in a 1D system, sequentially estimating phase saturations based on calculated pore species concentrations. Similarly, Korrani and Jerauld<sup>18</sup> utilized UTCHEM and PHREEQC to model wettability change in sandstone and carbonate rocks by estimating interfacial forces through surface and zeta potentials, ultimately calculating relative permeability. Moreover, Qiao et al.<sup>16</sup> and Sharma and Mohanty<sup>13</sup> also modeled wettability change in macro- and microscales, respectively, using UTCHEM-PHREEQC. However, these models have limitations in terms of considering only specific aspects or neglecting certain interfacial system complexities.

Jadhawar et al.<sup>19</sup> used the triple-layer surface complexation model and DLVO theory to analyze the effects of parameters such as polymer concentration, temperature, pH, and salinity on LSWF/LSP rheology. Using CMG-STARs and PHREEQC, they interpolated modified relative permeabilities from the measured (or simulated) maximum energy barrier in the polymer–brine–rock interfaces, thereby upscaling and analyzing wettability alteration occurring during LSWF,<sup>20</sup>

while on the MRST platform, Al-Shalabi et al.<sup>14</sup> coupled MRST with PHREEQC to model the geochemical role of LSP flooding, considering the sensitivity of the polymer (HPMA) and its impact on breakdown and lower displacement recovery factor in high-salinity conditions. Moreover, on MRST-PHREEQC, Hassan et al.<sup>21–23</sup> also modeled the polymer–brine–rock (PBR) system interaction and its impact on LSP performance as influenced by reservoir parameters such as salinity/hardness, polymer hydrolysis, rock composition/permeability, and temperature. These studies focused on the resultant polymer rheological impact (adsorption and viscosity effects). However, a direct wettability role, as modeled in previous approaches, has not yet been developed for LSWF/LSP in MRST.<sup>24</sup> Therefore, there is a need for a UTCHEM, ECLIPSE, and MRST model that offers an upscaled or field-scale, multidimensional PHREEQC-coupled model with a comprehensive COBR (crude oil–brine–rock) system complexation. Such an enhancement would significantly improve the capacity of these modeling toolboxes to investigate these EOR techniques robustly and reliably on the reservoir scale. This ultimately improves the design and management of productivity in mature oilfields, particularly carbonate oil reservoirs.

In this study, the coupled model used MRST's polymer model, which was originally developed by Bao et al.<sup>25</sup> and improved with the salinity effect on the LSP by Al-Shalabi et al.<sup>14</sup> The objective of this model is to simulate the wettability mechanism of low-salinity waterflooding (LSWF) and LSP in carbonate oil reservoirs, as previously modeled on MATLAB by Elakneswaran.<sup>15</sup> The coupled model considers the hydro-geochemical interactions of aqueous, oleic, and mineral phases in the crude oil–brine–rock (COBR) system, estimating the total oil adsorption and wettability indices of the rock. The relative permeabilities in MRST are modified based on these data. A detailed description of the base polymer model and the coupled model is provided, highlighting the improvements and enhancements made. The validation approach is outlined, and the results of the model's performance against core-scale experimental data for both single- and multiphase flooding scenarios are presented.

Furthermore, the outcomes of applying the model to field-scale LSWF/LSP modeling and simulation are presented, providing insights into the effectiveness of these processes in realistic reservoir conditions. The effects of reservoir permeability heterogeneity on LSWF/LSP are also investigated and discussed, shedding light on the challenges and opportunities associated with varying permeability distributions. Importantly, this study represents the first application of an MRST-PHREEQC model to upscale the wettability mechanism of low-salinity flooding in carbonate oil reservoirs. The findings presented contribute to a better understanding of LSWF/LSP processes and their potential implications for optimizing oil recovery in carbonate oil reservoirs.

## 2. MODEL DESCRIPTION

**2.1. Polymer Model.** This model implements a two-phase (i.e., oil and water) version of MRST's black-oil model for a recovery process in which polymer injection is performed.<sup>24,25</sup> In black-oil formulation, hydrocarbons exist as either liquid or gas under surface and reservoir conditions. At reservoir conditions, part of the oil and gas may vaporize or dissolve to form part of the oleic and gaseous phases, respectively.<sup>25</sup> This subsection explains the flow equation formulations for the

chemical and physical interactions of aqueous, oleic, and polymer phases (developed for MRST by Bao et al.<sup>14</sup>) and chemical species incorporated in this work, through eqs 1–13 and 14, respectively. Generally, the continuity equation for the injection/recovery process of any phase is described as

$$\partial t(\Phi b_\alpha S_\alpha) + \nabla \cdot (b_\alpha v_\alpha) = (b_\alpha q_\alpha) \quad (1)$$

where  $\Phi$  represents the rock's porosity and  $S$ ,  $b$ ,  $v$ , and  $q$  are the saturation, formation volume factor, and volumetric and source terms for a given phase  $\alpha$ . The Darcy flux equation is used to obtain the volumetric flux of each phase. The flux term depends on the phase's density ( $\rho_\alpha$ ), saturation ( $S_\alpha$ ), viscosity ( $\mu_\alpha$ ), including the overall pressure drop ( $\nabla p$ ), and effective ( $K$ ) and relative permeabilities ( $k_r$ ) and the influence of gravity on the flow ( $\nabla z$ ).

$$v = \frac{k_r}{\mu} K (\nabla p - \rho g \nabla z) \quad (2)$$

The primary mechanism of adding a polymer to the injection water is to raise its viscosity and decrease its reservoir mobility, which results in increasing the sweep/displacement efficiency of the flooding. Adversely, however, the polymer adsorbs onto the mineral surface, reducing the accessible pore space. The mass balance of the polymer solution, therefore, is modeled as

$$\partial t(\Phi(1 - s_{ipv})b_w s_w c_p) + \partial t(\rho_r(c_{ad}(1 - \Phi) + (\nabla \cdot (b_w v_p c_p))) = (b_w q_w c_p) \quad (3)$$

where  $s_{ipv}$  and  $c_{ad}$  account for the inaccessible pore volume and adsorption for the polymer component,  $c_p$ , respectively. Moreover, the modification of phase volumetric fluxes based on the resultant rheological effect of the polymer in water is considered through reduced mobility and effective viscosity terms and thus given as

$$v_w = -\frac{k_{rw}(s_w)}{\mu_{w,eff}(c_p)R_k(c_p)} K (\nabla p_w - \rho_w g \nabla z) \quad (4)$$

$$v_p = -\frac{k_{rp}(s_w)}{\mu_{p,eff}(c_p)R_k(c_p)} K (\nabla p_p - \rho_w g \nabla z) \quad (5)$$

The permeability reduction factor given in eq 6 is obtained as a function of polymer concentration and the residual reduction factor (RRF), which is a ratio of water before and after polymer flooding. Further, depending on polymer mixing and concentrations, the effective viscosities of water and polymer are calculated as given in eqs 7 and 8

$$R_k(c_p, c_{p,max}) = 1 + (RRF - 1) \frac{C_{ad}(c_p c_{p,max})}{c_{ad,max}} \quad (6)$$

$$\mu_{p,eff} = \mu_{fm}(c_p)^w \cdot \mu_p^{(1-w)} \quad (7)$$

$$\mu_{w,eff} = \frac{m_\mu(c_p)^w \mu_w}{1 - \bar{c} + \frac{m_\mu(c_p)^w}{m_\mu(c_p)^w}} (c^*)^{1-w} \quad (8)$$

The terms  $\mu_{fm}$  and  $m_\mu$  are a fully mixed polymer solution expression and a viscosity multiplier, respectively,  $\bar{c}$  and  $c^*$  are the normalized and maximum concentrations for the polymer, respectively, and  $w$  denotes its extent of mixing.

Further considerations are taken to account for the physical impact of the near-wellbore high shear rate and salinity effect on the polymer. To modify the shear rate, the shear viscosity modifier ( $z$ ) is calculated based on a user-defined shear rate multiplier ( $m_{sh}$ ) and  $m_\mu$  as follows

$$z = \frac{1 + (m_\mu - 1)m_{sh}}{m_\mu} \quad (9)$$

which is used to determine the adjusted sheared viscosities ( $\mu_{w,sh}$  and  $\mu_{p,sh}$ ) by multiplying it with the previously attained effective viscosities as

$$\mu_{w,sh} = (\mu_{w,eff})z \quad (10)$$

$$\mu_{p,sh} = (\mu_{p,eff})z \quad (11)$$

Then, to get the sheared volumetric fluxes ( $v_{w,sh}$  and  $v_{p,sh}$ ), normalized viscosities are divided by the shear viscosity multiplier in eqs 12 and 13. This study focused more on crude oil–brine–rock (COBR) system interactions and scale-up of the resultant role of salinity in wettability alteration during LSWF and LSP injection and less on the polymer–brine–brine (PBR) system. The geochemical interactions of polymers only influence the LSP process, given that polymers are not directly linked with the impacts of crude oil adsorption/desorption but rather improve water mobility. Therefore, for the LSP, we have considered the effect of salinity on the HPMA polymer by incorporating a viscosity multiplier that reflects normal viscosity at normal salinity and incremental change over an increase in salinity—essentially the divalent cations and PDIs by extension—as modeled by Al-Shalabi et al.<sup>14</sup>

$$v_{w,sh} = \frac{v_w}{z} \quad (12)$$

$$v_{p,sh} = \frac{v_p}{z} \quad (13)$$

**2.2. Geochemistry and Polymer Model.** In this coupled model, chemical species, i.e., sulfate, chloride, etc., transported in the aqueous phase are modeled by the addition of the term  $c_s$  in the phase continuity equation. A species  $S$  component mass balance then becomes

$$\frac{\partial}{\partial t}(\phi b_w s_w c_s) + \nabla \cdot (b_w v_w c_s) = b_w q_w c_s \quad (14)$$

The model's COBR system surface complexation considers a carbonate and oil surface interacting directly and via brine complexes, and the required reactions' kinetic data are adopted from the study of Elakneswaran.<sup>15</sup> Oil interacts with brine through asphaltene and resin's COOH carboxylic group; the mineral phase dissociates and interacts with cations such as  $H^+$  to form  $CaOH_2^+$  and  $CO_3^-$  that further form complexes with brine divalent ions—the interactions are mainly influenced by the crude oil's acidity, so basicity influence (e.g., by the amine group) is not included here.<sup>26,27</sup> These interactions are summarized in Table 1 below. The extent of oil adsorption on the calcite surface is estimated through quantification of the COOH group complexes given in Table 2.

Based on the reservoir's temperature ( $T$ ) and gas constant ( $R$ ), COOH complexes for negative (calcite<sup>-</sup>...oil<sup>+</sup>) and positive (calcite<sup>+</sup>...oil<sup>-</sup>) calcite surfaces are calculated as given in eqs 15 and 16, respectively.<sup>15,26</sup> The oil ( $\tau_{o/w}$ ) and calcite

**Table 1. Interfacial Interaction Complexation Equations and Equilibrium Constants of Calcite, Oil, and Brine Interfaces<sup>a</sup>**

equations	log $K_{@25^{\circ}\text{C}}$
$-\text{COOH} \leftrightarrow -\text{COO}^- + \text{H}^+$	$(0.0491 \times \log(\text{AN})) - 5.5461$
$-\text{COO}^+ + \text{Ca}^{2+} \leftrightarrow \text{COOCa}^+$	-4.8
$-\text{COO}^- + \text{Mg}^{2+} \leftrightarrow \text{COOMg}^+$	-4.
$>\text{CaOH} + \text{H}^+ \leftrightarrow \text{CaOH}_2^+$	15
$>\text{CO}_3\text{H} \leftrightarrow \text{CO}_3^- + \text{H}^+$	-7.3
$>\text{CO}_3^- + \text{Ca}^{2+} \leftrightarrow \text{CO}_3\text{Ca}^+$	-6.45
$>\text{CO}_3^- + \text{Mg}^{2+} \leftrightarrow \text{CO}_3\text{Mg}^+$	-6.15
$>\text{CaOH} + \text{SO}_4^{2-} \leftrightarrow \text{CaOH}(\text{SO}_4^-)$	14.75

<sup>a</sup>AN: acid number.**Table 2. Complexes of Carboxylic Acid Interactions with Various Brine and Calcite Surface Species Used in Oil Adsorption Analysis**

equations
$-\text{COO}^- + \text{CaOH}_2^+ \leftrightarrow \text{CaOH}_2(\text{COO})$
$-\text{COO}^- + \text{CO}_3\text{Ca}^+ \leftrightarrow \text{CO}_3\text{Ca}(\text{COO})$
$-\text{COO}^- + \text{CO}_3\text{Mg}^+ \leftrightarrow \text{CO}_3\text{Mg}(\text{COO})$
$>\text{COOCa}^+ + \text{CO}_3^- \leftrightarrow \text{COOCa}(\text{CO}_3)$
$>\text{COOCa}^+ + \text{CaOH}_2\text{SO}_4^- \leftrightarrow \text{COOCa}(\text{CaOH}_2\text{SO}_4)$
$>\text{COOMg}^+ + \text{CO}_3^- \leftrightarrow \text{COOMg}(\text{CO}_3)$
$>\text{COOMg}^+ + \text{CaOH}_2\text{SO}_4^- \leftrightarrow \text{COOMg}(\text{CaOH}_2\text{SO}_4)$

$(\tau_{c/w})$  surface  $\zeta$ -potentials are also spatiotemporal values in each of these reactions with their specific reaction constants ( $K$ ). The data of total oil adsorption at any given time and

space in the reservoir ( $x, t$ ) after flooding are then divided by the same data estimated at the initial state (i.e., just before flooding), and the results are subtracted from 1 (i.e., the reservoir's oil-wet state) to get the wettability alteration index ( $w$ ) as given in eq 17

$$(\text{calcite}^- \dots \text{oil}^+) = \frac{K_-[(\text{oil})^+][(\text{calcite})^-]}{\exp\left(\frac{-F}{RT}(\tau_{c/w} - \tau_{o/w})\right)} \quad (15)$$

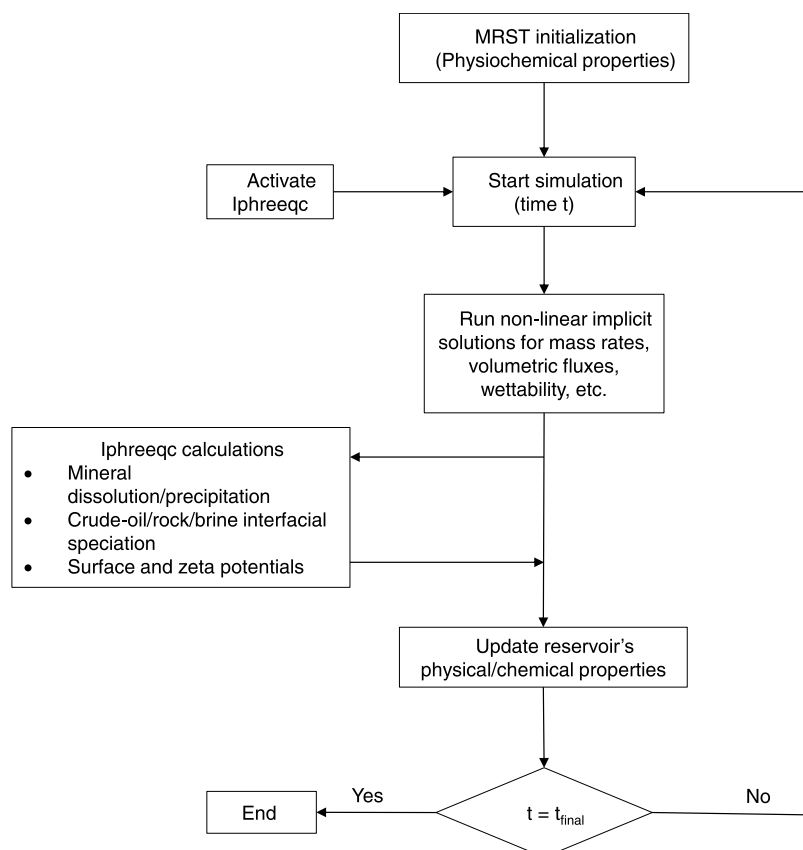
$$(\text{calcite}^+ \dots \text{oil}^-) = \frac{K_+[(\text{oil})^-][(\text{calcite})^+]}{\exp\left(\frac{-F}{RT}(\tau_{c/w} - \tau_{o/w})\right)} \quad (16)$$

$$w = 1 - \frac{[(\text{calcite}^+ \dots \text{oil}^-) + (\text{calcite}^- \dots \text{oil}^+)]_{(x,t)}}{[(\text{calcite}^+ \dots \text{oil}^-) + (\text{calcite}^- \dots \text{oil}^+)]_{\text{initial}}} \quad (17)$$

Furthermore, as the key input parameter into MRST from geochemistry data, the index is subsequently used in eqs 18 and 19, with the measured end-point relative permeabilities at oil-wet ( $k_{\text{rw}_{\text{ow}}}$  and  $k_{\text{ro}_{\text{ow}}}$ ) and water-wet ( $k_{\text{rw}_{\text{ww}}}$  and  $k_{\text{ro}_{\text{ww}}}$ ) conditions, to get the intermediary end-point relative permeabilities ( $k_{\text{rw}_{\text{ep}}}$  and  $k_{\text{ro}_{\text{ep}}}$ ).<sup>16</sup> These values are then the new inclusions in the MRST's relative permeability ( $k_{\text{rw}}$  and  $k_{\text{ro}}$ ) calculations in eqs 20 and 21, which are determined as the Corey model's monomial functions of phase saturation ( $S_{\alpha}^n$ ), where  $\alpha$  and  $n$  denote the phase and exponents, respectively

$$k_{\text{rw}_{\text{ep}}} = wk_{\text{rw}_{\text{ow}}} + (1 - w)k_{\text{rw}_{\text{ww}}} \quad (18)$$

$$k_{\text{ro}_{\text{ep}}} = wk_{\text{ro}_{\text{ow}}} + (1 - w)k_{\text{ro}_{\text{ww}}} \quad (19)$$

**Figure 1.** MRST-PHREEQC-coupled model simulation flowchart sequence implemented in this study.

$$k_{rw} = k_{rw\_ep} * s_w^n \quad (20)$$

$$k_{ro} = k_{ro\_ep} * s_o^n \quad (21)$$

The summary of the coupled model is provided in Figure 1 below. First, the initialization process begins by incorporating the reservoir petrophysical data and boundary conditions into MRST. Simultaneously, the formation geochemical state is initialized through the utilization of the initial solution, phase, and surface complexation simulations in PHREEQC. The resulting data are stored in MRST's state and used to calculate secondary parameters such as the wettability index. Second, the state object, schedule, and boundary conditions (wells) are passed onto MRST's nonlinear solver, which proceeds to perform the physical implicit solutions for the first time step (0). Subsequently, a cell-wise PHREEQC geochemical simulation is conducted for the current time step. In 1D simulations, the process begins from cell [1,1,1] and progresses to cell [n, 1, 1], where n represents the last cell in the reservoir. However, in 3D calculations, the process is looped based on the *G.cells.indexMap*, which assigns an index to each cell in the grid.

The PHREEQC lines accumulated during the simulation are then executed by using the designated AccumulateLine and RunAccumulated functions. The results obtained from these physical and chemical solutions are passed back into the state, leading to the update and re-estimation of parameters such as oil adsorption, wettability index, and relative permeabilities. Subsequently, these parameters are utilized in the previously explained equations to compute the mobilities of the reservoir and surface phases. This iterative process continues until the final injection period is reached. Since MRST is written on MATLAB, simulating with any module available on it requires describing the problem on the input script. Thus, one can either copy an available script template and modify it based on the problem to be solved or write an entirely new script once each key-building element of the model is understood. Reservoir petrophysical properties, such as crude oil characteristics, reservoir temperature, salinity, porosity and permeability, schedule, and boundary conditions, are some of the basic parameters that are specific to reservoir models.

### 3. RESULTS AND DISCUSSION

**3.1. Core-Scale Validation.** **3.1.1. Single Phase.** In the first case, core flooding experiment data from a study by Strand et al.<sup>28</sup> were used to compare the performance of the coupled model against PHREEQC. In this case, the experiment was carried out at 20 °C to examine the affinity of Ca<sup>2+</sup> and Mg<sup>2+</sup> ions toward the carbonate surface. The core was initially saturated with NaCl solution (Table 3), and a 0.1 mL/min rate of low-salinity injection was performed. The simulation configurations and reservoir petrophysical properties are listed in Table 4.

The results of the simulation are shown in the following figures. In Figure 2, the model prediction of ion profiles was graphed against that simulated in PHREEQC as a function of pore volumes injected (PVI). The prediction changes in the effluent concentration in PHREEQC, with a rise in Ca<sup>2+</sup> and Mg<sup>2+</sup> and a drop in Na<sup>+</sup> and Cl<sup>-</sup> after 0.5 PVI, were well matched by the model. Also, as more than 1.5 PVI were injected, the ionic profiles dropped/rose to the injection levels, which was highly accurately predicted by the model.

**Table 3. Composition of Injection and Formation Water of a Single-Phase Core Flooding Experiment Used to Compare the Model against PHREEQC**

ion	injection (mmol/L)	formation (mmol/L)
Ca <sup>2+</sup>	13	0
Mg <sup>2+</sup>	13	0
Na <sup>+</sup>	504	573
Cl <sup>-</sup>	556	573
pH	6.9	6

**Table 4. Petrophysical Parameters and Reservoir Conditions of the Core Sample Used in Model-PHREEQC Comparison**

parameter	value	unit
dimension	[0.0491, 0.0335, 0.0335]	meter
permeability	2.7	millidarcy
porosity	24.7	percent
permeability exponent	[1, 1]	
water surface density	1000	kg/m <sup>3</sup>
well radius	0.002	meter
temperature	20	celsius
water saturation	100	percent

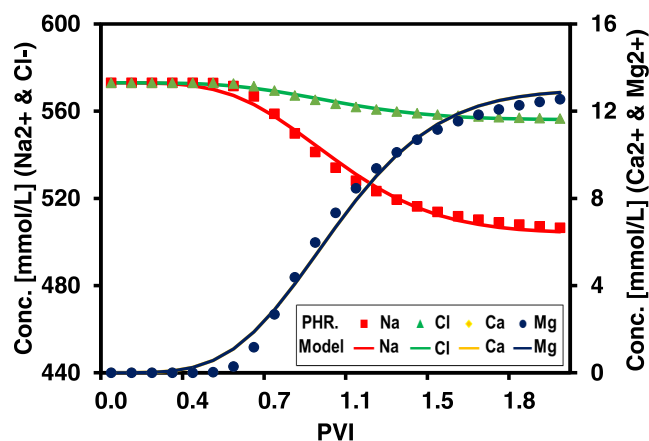


**Figure 2.** Comparison of the model and PHREEQC ion profile prediction.

Further, in Figure 3, the data of Ca<sup>2+</sup> and Mg<sup>2+</sup> obtained in the experiment were matched with the model's prediction. The graph shows the relative ionic concentration profiles for these

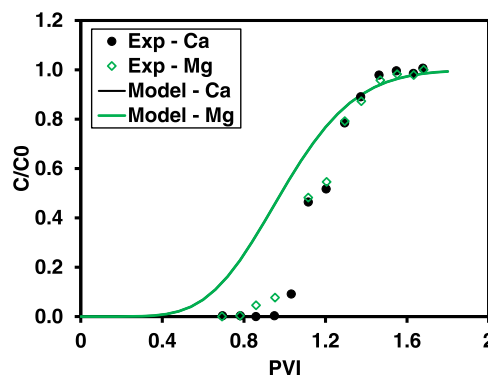


**Figure 3.** Predicted relative concentrations compared with experimental data.

two cations as a function of PVI, where the final values were divided by the initial values ( $C/C_0$ ). The profiles rose in the model after 0.5 PVI, while in the experiment, there was a delay of 0.3 PVI as the rise started after 0.8 PVI. The difference was due to MRST's upwind solutions, which was not the case in the experiment process. However, this dissimilarity was reduced after 1.2 PVI as the relative profiles started to match and continued for the remainder of the injection.

In the second case, a single-phase core flooding experiment of Chandrasekhar et al.,<sup>29</sup> which was carried out at 120 °C and 55 psi, was simulated by the model to history-match the measured effluent concentrations. The experiment equilibrated the core with formation salinity under the stated conditions, and a low-salinity injection was carried out at 0.02 mL/min rate. Then, the effluent concentrations were measured. Tables 5 and 6 provide the brine concentration, reservoir data, and

**Table 5. Composition of Injection and Formation Water Used in the Model's Verification against an Experimental Single-Phase Core Flooding Result**

ion	Injection (mmol/L)	formation (mmol/L)
Ca <sup>2+</sup>	13.25	334.5
Mg <sup>2+</sup>	65.42	138.1
Na <sup>+</sup>	578.2	2091
Cl <sup>-</sup>	785	3611
SO <sub>4</sub> <sup>2-</sup>	37.99	2.67
H <sup>+</sup>	1 × 10 <sup>-7</sup>	1 × 10 <sup>-7</sup>

**Table 6. Core Sample Dimensions, Petrophysical Properties, and Conditions**

parameter	value	unit
dimension	[0.153, 0.0337, 0.0337]	meter
permeability	25	millidarcy
porosity	17	percent
permeability exponent	[1, 1]	
water surface density	1000	kg/m <sup>3</sup>
well radius	0.005	meter
temperature	120	celsius
water saturation	99.9	percent

injection configurations. The simulation results showed a highly accurate match of the effluent ionic profiles (refer to Figure 4). The Cl<sup>-</sup> formation concentration was charge-balanced in the simulation for smooth convergence in PHREEQC, and this showed a slightly lower prediction model Cl<sup>-</sup> for the first 1 PVI. However, overall, the model's

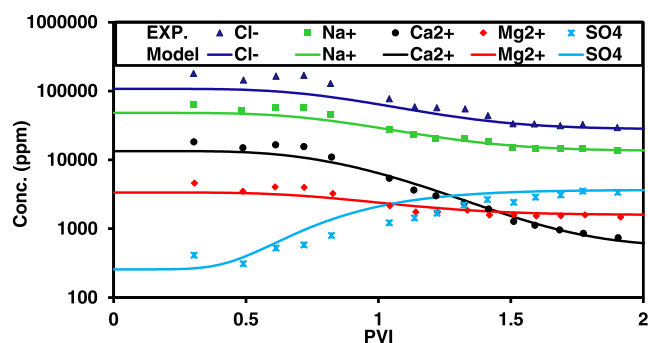


**Figure 4.** Predicted effluent concentrations of salinity ions compared with experimental data.

prediction and the experiment indicated a good match in all the ionic profiles.

**3.1.2. Multiphase.** To further validate the model, we simulated a two-phase core flooding experiment performed by Chandrasekhar.<sup>30</sup> A limestone core of 26.4% porosity and 7.6 permeability was aged in the experiment with 2.45 mg of KOH/g of crude oil, producing a 68% oil saturation (see Table 7); three brine solutions were injected at a constant rate of

**Table 7. Physical Parameters of the Core Sample, Crude Oil Properties, and Reservoir Conditions of the Two-Phase Flooding Experimental Process Used to Validate the Model**

parameter	value	unit
dimension	[0.0529, 0.0173, 0.0173]	meter
permeability	7.6	millidarcy
porosity	26.4	percent
permeability exponent	[1, 1]	
water surface density	1000	kg/m <sup>3</sup>
oil surface density	860	kg/m <sup>3</sup>
well radius	0.005	meter
temperature	120	celsius
water saturation	32	percent
oil saturation	68	percent
acid number	2.45	mg KOH/g

**Table 8. Composition of Formation Water (FW), Injected Seawater (SW), and Diluted SW Floods (SW/2 and SW/10) Used in the Simulation**

ion (mmol/L)	FW	SW	SW/2	SW/10
Ca <sup>2+</sup>	2120.5	626.6	313.3	62.7
Mg <sup>2+</sup>	330.7	69.68	34.83	6.97
Na <sup>+</sup>	131	13.6	6.8	1.36
Cl <sup>-</sup>	4007.8	721.7	360.85	72.2
SO <sub>4</sub> <sup>2-</sup>	2.51	36	18	3.6

19.7 mL/min (refer to Table 8). The injection sequence started with 12 PV of seawater (SW), followed by 26 PV of two times diluted seawater (SW/2) and ended with 10 PV of ten times diluted seawater (SW/10). The adopted end-point relative permeabilities in the model are listed in Table 9. The

**Table 9. End-Point Relative Permeabilities Used in the Multiphase Modeling**

end-point rel. perm.	oil-wet	water-wet
$k_{rw}$	0.75	0.2
$k_{ro}$	0.4	0.8

results of ionic profiles, pH, and oil recovery predicted by the model are compared to the experimental data in Figures 5 and 6. The ion compositions are plotted relative to their initial concentrations against PVI (Figure 5A–C); as can be seen, the model provides a close fit to the experimental observations. Moreover, while there's some degree of variation in pH and oil recovery, particularly on the sensitivity of recovery to the injection sequence, the oil incremental recovery, pH trend, and ultimate recovery factor of 66% are well matched by the model prediction. The notable inadequacy in the model's predicted oil recovery factor (Figure 6A) is predetermined by the

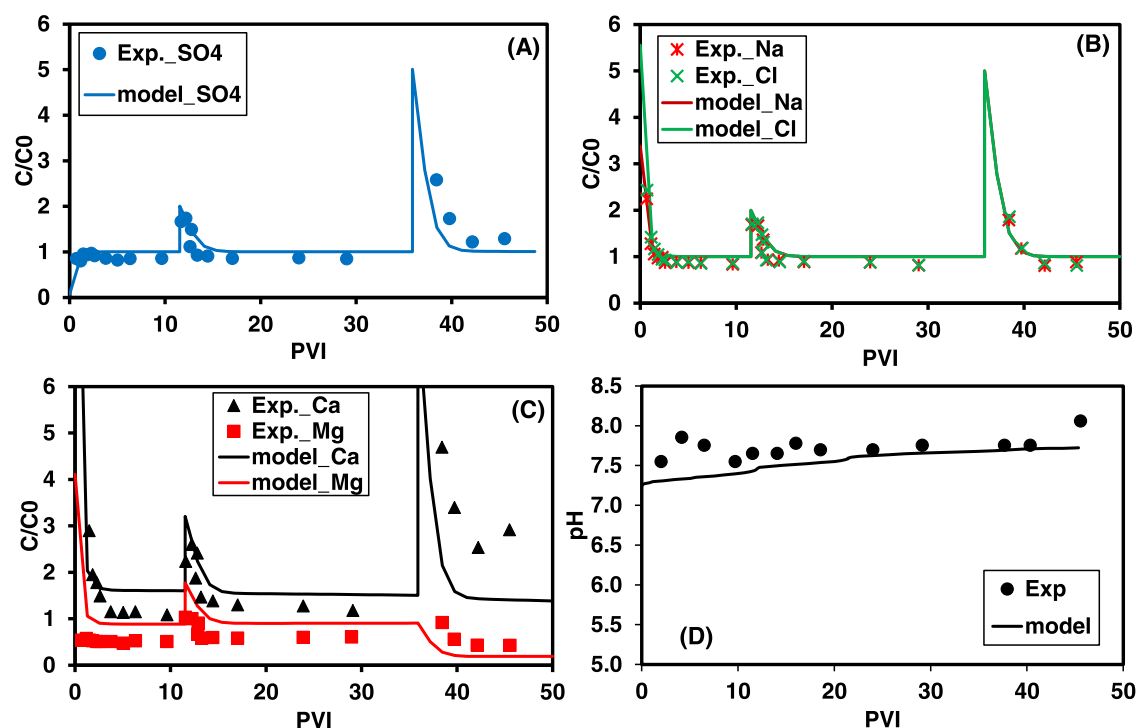


**Figure 5.** Predicted effluent concentration of sulfate (A), sodium and chloride (B), calcium and magnesium (C), and pH (D) compared with experimental data.

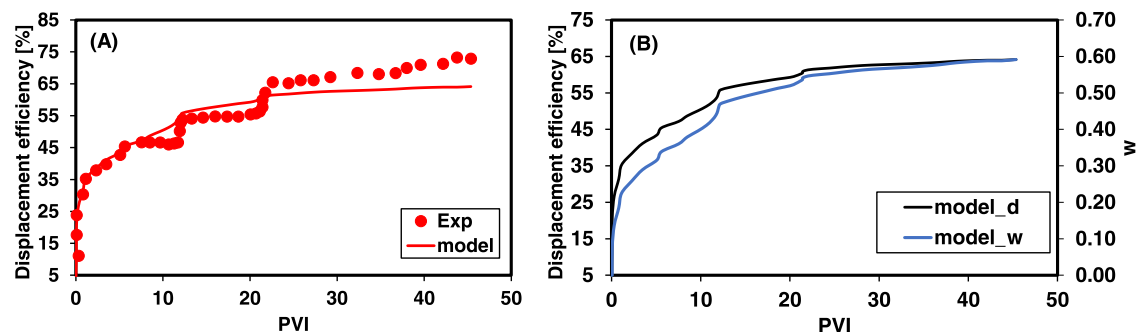


**Figure 6.** Predicted oil recovery efficiency compared with the experiment (A) and fitting of the predicted displacement factor and wettability index (B).

estimated wettability index, and these two match adequately, as seen in Figure 6B.

**3.2. Field-Scale Simulation.** **3.2.1. Low-Salinity and Polymer Flooding.** To further validate the potency of the coupled model, low-salinity waterflooding (LSWF) and low-salinity polymer flooding (LSP) were modeled with experimental data from the study of Al-Hammadi et al.<sup>31</sup> (refer to Table 10). In their study, a carbonate oil reservoir core, saturated with the crude oil of 2.18 cP, 0.85 wt % asphaltene, and 0.7 mg of KOH/g of AN, was flooded in secondary mode with a high salinity or formation brine (FW) prepared based on Middle Eastern oil reservoir salinity. A 200 times diluted FW (FW/200) with less than 10,000 ppm salinity was injected to investigate the tertiary LSWF performance. In the modeling, a third sequential flooding was considered for LSP. The diluted FW/200 added with 2 kg/m<sup>3</sup> HPAM was used. Other simulation parameters are given in Table 11. Figure 7 shows that a maximum of 9% original oil in place (OOIP) could be recovered in the field application of FW in this oil reservoir, a 50% lower recovery than what was achieved in the core

**Table 10. Composition of Injection and Formation Water Used in the Macroscale Simulation of LSWF/LSP**

ion (mmol/L)	FW	FW/200	FW/200P <sup>a</sup>
Ca <sup>2+</sup>	462.3	2.311	2.311
Mg <sup>2+</sup>	68.8	0.344	0.344
Na <sup>+</sup>	2576.8	12.89	12.89
Cl <sup>-</sup>	3626.85	18.13	18.13
SO <sub>4</sub> <sup>2-</sup>	3.91	0.02	0.02
TDS	208 600		

<sup>a</sup>FW/200P: 200 times diluted formation water (FW) with 2 kg/m<sup>3</sup> HPMA polymer.

flooding experiment. However, the 3% additional OOIP recovery by LSWF accurately matches the 2–3% obtained in the experiment and in other studies.<sup>32,33</sup> Moreover, LSP injection exhibited the possibility of a further 2% OOIP incremental recovery. This is 8% less than the average attained in carbonate oil core flooding with seawater; however, this may

**Table 11. Formation and Flooding Simulation Data**

parameter	value	unit
dimension	[100, 50, 20]	meter
permeability	100	millidarcy
porosity	30	percent
permeability exponent	[1, 1]	
water surface density	1000	kg/m <sup>3</sup>
well radius	0.12	meter
temperature	50	celsius
water saturation	20	percent
production period	1	year
oil density	860	kg/m <sup>3</sup>
oil viscosity	5	cp
pressure	330	bars
acid number	0.7	mg KOH/g

be due to the low  $\text{SO}_4^{2-}$  concentration in diluted FW used in the modeled LSP.<sup>34</sup>

Furthermore, based on oil production rates (Figure 8), the peak oil recovery rate was rapidly reached within 0.2 PVI during the FW injection ( $31 \text{ m}^3/\text{day}$ ). This afterward dropped to  $6\text{--}8 \text{ m}^3/\text{day}$  for an additional 0.3 PVI (40 days) before the switch to LSWF at an average of  $4 \text{ m}^3/\text{day}$  for 0.5 PVI (67 days). Also, the subsequent LSP flood ran at a slightly lower average of  $3\text{--}3.5 \text{ m}^3/\text{day}$ . This fluctuation is mainly due to the reservoir pressure drop, which was initially at 330 bar, below the production well's 250 bar bottom hole pressure (BHP), but also due to the flooding phase geochemical influence. Thus, FW cumulatively produced 60% of the oil recovered, while LSWF and LSP recovered additionally 20 and 19%, respectively (refer to Figure 8A).

**3.2.2. Heterogeneous Permeability Effect.** The simulation carried out in the preceding section was further modeled by considering a more practical layered and anisotropic permeability in the same reservoir model. The absolute permeability was assumed to vary as 150, 200, and 100 mD

in the top, bottom, and middle sections, respectively (shown in Figure 9), while anisotropy was introduced by assuming horizontal ( $K_x$ ) and vertical ( $10K_z$ ) variation

$$K_x = 10K_z \quad (22)$$

Figure 10 shows the flooding simulation results of the heterogeneous model ( $K_{\text{aniso}}$ ) compared with the homogeneous model ( $K_{\text{iso}}$ ). While the FW flood oil recovery rates were similar in both models, the  $K_{\text{aniso}}$  peak rate was 77% higher. Also, the total oil production in  $K_{\text{aniso}}$  dropped by 4% and increased by 3 and 1% in FW, LSWF, and LSP, respectively. These results indicate the favorability of heterogeneity in reservoir permeability toward low-salinity flooding at field-scale application in carbonate oil reservoirs. This is consistent with a study by Al-Ibadi et al.,<sup>35</sup> where LSWF in a carbonate oil reservoir was modeled through a set of LSWF's wettability hysteresis on permeability. Also, note that the considered stratigraphic and anisotropic permeability distributions may not adequately represent the influence of LSWF in other permeability variations. The geology considered through a sandbox is moderately representative of the normal reservoir, which is usually intersected by faults and has petrophysical properties that vary exponentially over close distances. Nonetheless, the simulation agrees with LSWF and LSP laboratory core-scale data and field-scale results modeled with log-normal permeability distribution.<sup>34,35</sup>

#### 4. CONCLUSIONS

The purpose of our work was to integrate MRST with geochemistry to model and simulate the complex interactions between crude oil, rock, and brine during low salinity waterflooding (LSWF/LSP) at the reservoir scale. To achieve this, we used MRST's polymer model and PHREEQC. Based on the results of our numerical study, we drew the following conclusions:

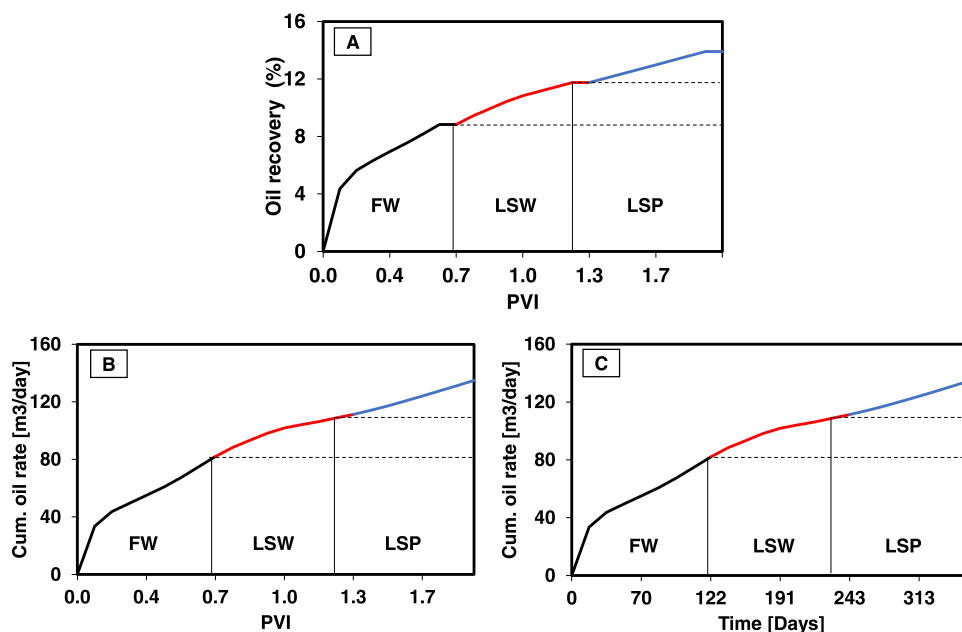


**Figure 7.** Predicted oil recovery (A) and cumulative oil recovery rates as functions of PVI (B) and time (C) for LSWF and LSP secondary/tertiary recovery.

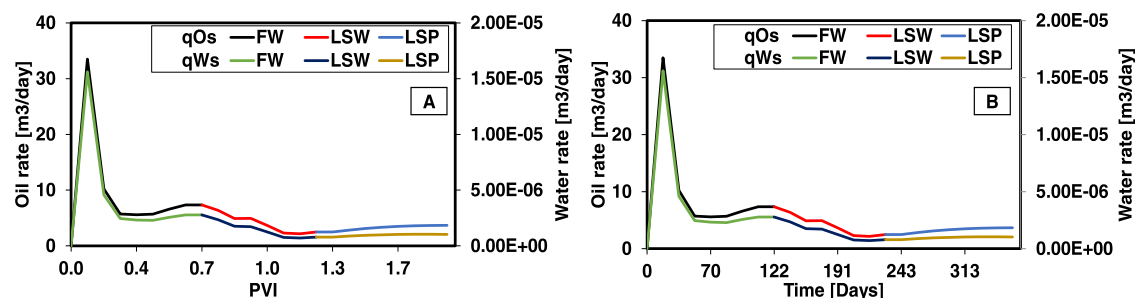


Figure 8. Oil and water surface rates vs PVI (A) and time (B) for LSWF and LSP secondary/tertiary recovery.

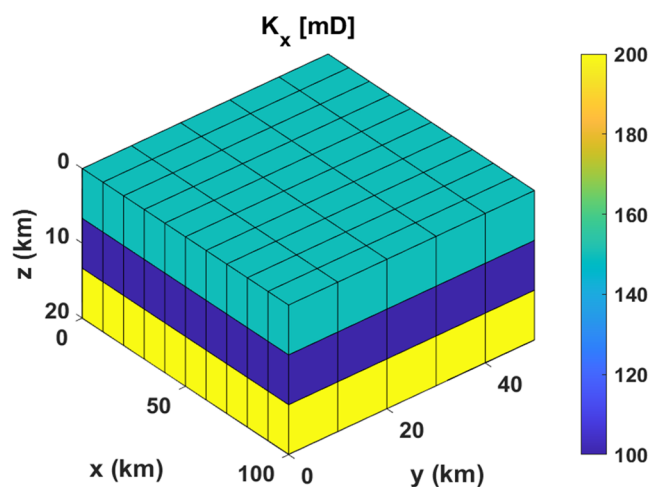


Figure 9. Modeled absolute permeability heterogeneity of a carbonate oil reservoir, with a stratigraphic range of 100–200 and 10 mD anisotropy in the x-z directions.

- (1) The polymer model of MRST was successfully extended and coupled with PHREEQC's aqueous, equilibrium, and surface complexation capabilities.
- (2) The coupled model was validated with core-scale single-phase and multiphase experimental flooding data with high accuracy in effluent ionic and oil recovery profiles.
- (3) The model's simulation of low-salinity waterflooding and polymer flooding exhibited additional tertiary oil recovery of 3 and 2%, respectively, which are within the range of reported core flooding and field results.
- (4) The simulation of sequential FW, LSWF, and LSP flooding indicated 61, 20, and 19% oil recovery when applied in secondary mode, but the results of FW were 50% off compared to regular core flooding due to upscaling limitations.
- (5) The modeling of vertical and anisotropic permeability heterogeneity effect showed a positive synergy with low-salinity floodings with a 4% drop and 3 and 1% increase in FW, LSWF, and LSP, respectively, a result trend reported in a previous carbonate core model.
- (6) These results demonstrated that the coupled model and its approach could be used in the field-scale inves-

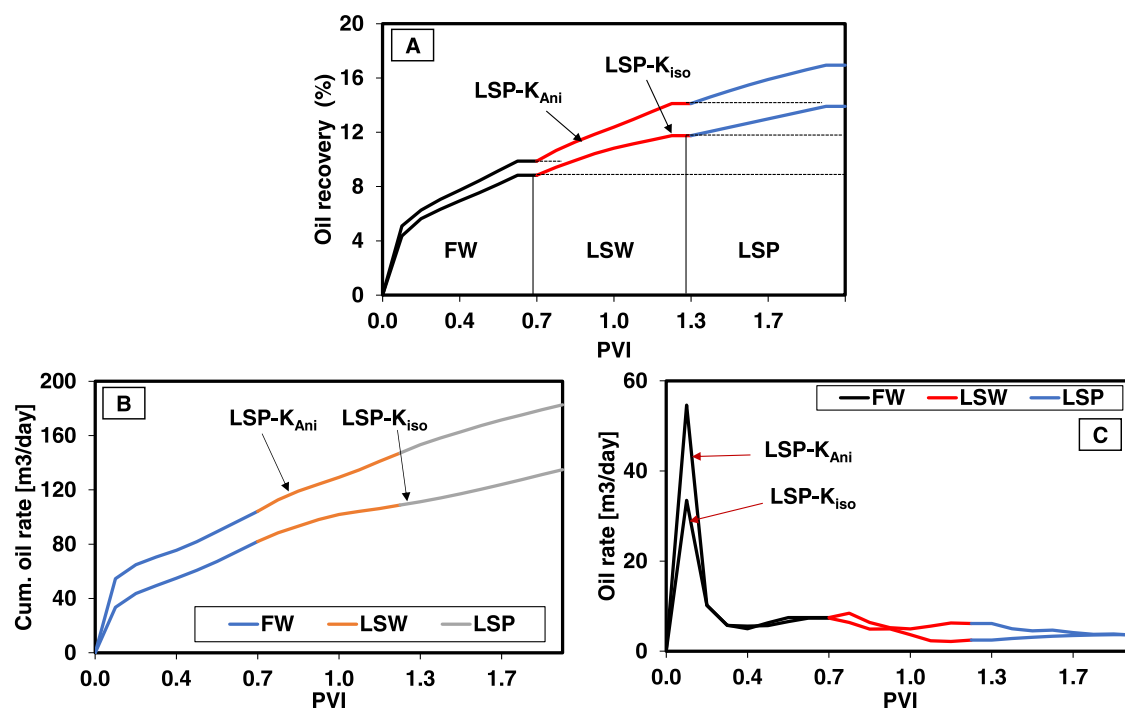


Figure 10. Comparison of oil recovery efficiency (A), cumulative oil recovery as a function of PVI (B), and oil recovery rates as a function of PVI (C) for FW, LSWF, and LSP in a carbonate oil reservoir.

tigations of LSW-based EOR in carbonate oil reservoirs, thus improving the capacity of performing these analyses robustly and reliably.

## ■ ASSOCIATED CONTENT

### Data Availability Statement

Data will be made available on request.

### SI Supporting Information

The Supporting Information is available free of charge at <https://pubs.acs.org/doi/10.1021/acsomega.3c10022>.

Field-scale, multiphase, and single-phase experimental and raw data (ZIP)

## ■ AUTHOR INFORMATION

### Corresponding Author

Yogarajah Elakneswaran – Division of Sustainable Resources Engineering Faculty of Engineering, Hokkaido University, Sapporo 060-8628, Japan; [orcid.org/0000-0001-5496-5551](https://orcid.org/0000-0001-5496-5551); Phone: +81-11-706-7274; Email: [elakneswaran@eng.hokudai.ac.jp](mailto:elakneswaran@eng.hokudai.ac.jp)

### Authors

Angelo Kennedy Lino Limaluka – Division of Cooperative Program for Resources Engineering Faculty of Engineering, Hokkaido University, Sapporo 060-8628, Japan; [orcid.org/0009-0003-9317-1692](https://orcid.org/0009-0003-9317-1692)

Naoki Hiroyoshi – Division of Sustainable Resources Engineering Faculty of Engineering, Hokkaido University, Sapporo 060-8628, Japan

Complete contact information is available at:

<https://pubs.acs.org/doi/10.1021/acsomega.3c10022>

### Author Contributions

A.K.L.L.: methodology, investigation, writing—original draft, and writing—review and editing. Y.E.: methodology, supervision, writing—review and editing, and funding acquisition. N.H.: supervision, writing—review and editing, and funding acquisition.

### Notes

The authors declare no competing financial interest.

## ■ ACKNOWLEDGMENTS

The author thanks the Ministry of Education, Culture, Sports, Science and Technology, Japan (MEXT), for the scholarship provided during this work.

## ■ REFERENCES

- (1) bp 2021 <https://www.bp.com/en/global/corporate/energy-economics/statistical-review-of-world-energy/primary-energy.html> (accessed on June 19, 2022).
- (2) IEA. Oil Market Report - April 2023 – Analysis - IEA 2023 <https://www.iea.org/reports/oil-market-report-april-2023> (accessed on June 09, 2023).
- (3) Fink, J. *Petroleum Engineer's Guide to Oil Field Chemicals and Fluids-Gulf Professional Publishing* (2021); Joe Hayton, 2021.
- (4) Afekare, D. A.; Radonjic, M. From Mineral Surfaces and Coreflood Experiments to Reservoir Implementations: Comprehensive Review of Low-Salinity Water Flooding (LSWF). *Energy Fuels* **2017**, *31* (12), 13043–13062.
- (5) Al-Kaabi, A.; Kokal, S. Enhanced oil recovery: challenges and opportunities 2023 [https://firstforum.org/wp-content/uploads/2021/05/Publication\\_00466.pdf](https://firstforum.org/wp-content/uploads/2021/05/Publication_00466.pdf) (accessed on June 09, 2023).

(6) Delamaide, E. *Is chemical EOR finally coming of age?*, IOR 2021 - 21st European Symposium on Improved Oil Recovery, 2021; pp 1–30 DOI: [10.3997/2214-4609.202133010/CITE/REFWORKS](https://doi.org/10.3997/2214-4609.202133010/CITE/REFWORKS).

(7) Gbadamosi, A.; et al. Recent advances on the application of low salinity waterflooding and chemical enhanced oil recovery. *Energy Rep.* **2022**, *8*, 9969–9996, DOI: [10.1016/j.egy.2022.08.001](https://doi.org/10.1016/j.egy.2022.08.001).

(8) Andrews, E.; Muggeridge, A.; Jones, A.; Krevor, S. Pore structure and wetting alteration combine to produce the low salinity effect on oil production. *Fuel* **2023**, *332*, No. 126155.

(9) Bigdeli, A.; Thyne, G.; Ulyanov, V. Low Salinity Water Flooding (LSWF), Can We Move Forward? The Economic Case. *J. Resour. Recovery* **2023**, *1* (1), 1002.

(10) Sarma, H. K.; Singh, N.; Belhaj, A. F.; Jain, A. K.; Gopal, G.; Srivastava, V. R. *A Lab-to-Field Approach and Evaluation of Low-Salinity Waterflooding Process for High-Temperature High-Pressure Carbonate Reservoirs*, Society of Petroleum Engineers - SPE Asia Pacific Oil and Gas Conference and Exhibition 2022, APOG 2022, Oct., 2022 DOI: [10.2118/210657-MS](https://doi.org/10.2118/210657-MS).

(11) Nguyen, N.; Dang, C.; Gorucu, S. E.; Nghiem, L.; Chen, Z. The role of fines transport in low salinity waterflooding and hybrid recovery processes. *Fuel* **2020**, *263*, No. 116542.

(12) Olabode, O.; Alaigba, D.; Oramabo, D.; Bamigboye, O. Modelling Low-Salinity Water Flooding as a Tertiary Oil Recovery Technique. *Modell. Simul. Mater.* **2020**, *2020*, No. 6485826, DOI: [10.1155/2020/6485826](https://doi.org/10.1155/2020/6485826).

(13) Sharma, H.; Mohanty, K. K. Modeling of low salinity waterflooding in carbonates: Effect of rock wettability and organic acid distribution. *J. Pet. Sci. Eng.* **2022**, *208*, No. 109624.

(14) Al-Shalabi, E. W.; Alameri, W.; Hassan, A. M. Mechanistic modeling of hybrid low salinity polymer flooding: Role of geochemistry. *J. Pet. Sci. Eng.* **2022**, *210*, No. 110013.

(15) Elakneswaran, Y. *Modelling the Impact of Surface Charge on Wettability Alteration in Low Salinity Waterflooding*, Proceedings - SPE Symposium on Improved Oil Recovery, 2022 DOI: [10.2118/209357-MS](https://doi.org/10.2118/209357-MS).

(16) Qiao, C.; Johns, R.; Li, L. Modeling Low-Salinity Waterflooding in Chalk and Limestone Reservoirs. *Energy Fuels* **2016**, *30* (2), 884–895.

(17) Kazemi Nia Korrani, A.; Sepehrmoori, K.; Delshad, M. Coupling IPHreeqc with UTCHEM to model reactive flow and transport. *Comput. Geosci* **2015**, *82*, 152–169.

(18) Korrani, A. K. N.; Jerauld, G. R. Modeling wettability change in sandstones and carbonates using a surface-complexation-based method. *J. Pet. Sci. Eng.* **2019**, *174*, 1093–1112.

(19) Saeed, M.; Jadhawar, P. Surface Complexation Modeling of HPAM Polymer-Brine-Sandstone Interfaces for Application in Low-Salinity Polymer Flooding. *Energy Fuels* **2023**, *37* (9), 6585–6600.

(20) Jadhawar, P.; Saeed, M. Low salinity water and polymer flooding in sandstone reservoirs: Upscaling from nano-to macro-scale using the maximum energy barrier. *J. Pet. Sci. Eng.* **2023**, *220*, No. 111247.

(21) Hassan, A. M.; Al-Shalabi, E. W.; AlAmeri, W.; Kamal, M. S.; Patil, S.; Shakil Hussain, S. M. *A Coupled Geochemical-Based Modeling Approach for Low Salinity Polymer (LSP) Injection: Effects of Salinity, Rock-Type, and Temperature on Polymer Rheology*, SPE Western Regional Meeting Proceedings, 2023 DOI: [10.2118/213049-MS](https://doi.org/10.2118/213049-MS).

(22) Hassan, A. M. et al. *Surface Complexation Modeling for Low Salinity Polymer (LSP) Injection in Carbonate Reservoirs Under Harsh Conditions*, Society of Petroleum Engineers - ADIPEC, ADIP 2023, Oct., 2023 DOI: [10.2118/216501-MS](https://doi.org/10.2118/216501-MS).

(23) Hassan, A. M. et al. *Novel Impressions of Hybrid Low Salinity Polymer (LSP) Injection: A Geochemical Modeling Study*, Society of Petroleum Engineers - ADIPEC, ADIP 2023, Oct., 2023 DOI: [10.2118/216197-MS](https://doi.org/10.2118/216197-MS).

(24) Lie, K.-A. *An Introduction to Reservoir Simulation Using MATLAB/GNU Octave*; Cambridge University Press, 2019 DOI: [10.1017/9781108591416](https://doi.org/10.1017/9781108591416).

- (25) Bao, K.; Lie, K. A.; Møyner, O.; Liu, M. Fully implicit simulation of polymer flooding with MRST. *Comput. Geosci* **2017**, *21* (5–6), 1219–1244.
- (26) Takeya, M.; Shimokawara, M.; Elakneswaran, Y.; Nawa, T.; Takahashi, S. Predicting the electrokinetic properties of the crude oil/brine interface for enhanced oil recovery in low salinity water flooding. *Fuel* **2019**, *235*, 822–831.
- (27) Takeya, M.; Shimokawara, M.; Elakneswaran, Y.; Okano, H.; Nawa, T. Effect of Acid Number on the Electrokinetic Properties of Crude Oil during Low-Salinity Waterflooding. *Energy Fuels* **2019**, *33* (5), 4211–4218.
- (28) Strand, S.; Austad, T.; Puntervold, T.; Høgenesen, E. J.; Olsen, M.; Barstad, S. M. F. Smart Water' for oil recovery from fractured limestone: A preliminary study. *Energy Fuels* **2008**, *22* (5), 3126–3133.
- (29) Chandrasekhar, S.; Sharma, H.; Mohanty, K. K. Dependence of wettability on brine composition in high temperature carbonate rocks. *Fuel* **2018**, *225*, 573–587.
- (30) Chandrasekhar, S. Wettability Alteration with Brine Composition in High Temperature Carbonate Reservoirs 2013 <https://repositories.lib.utexas.edu/bitstream/handle/2152/22657/CHANDRASEKHAR-MASTERSREPORT-2013.pdf?sequence=1&isAllowed=y> (accessed on September 26, 2022).
- (31) AlHammadi, M.; Mahzari, P.; Sohrabi, M. Fundamental investigation of underlying mechanisms behind improved oil recovery by low salinity water injection in carbonate rocks. *Fuel* **2018**, *220*, 345–357.
- (32) Austad, T.; Shariatpanahi, S. F.; Strand, S.; Black, C. J. J.; Webb, K. J. Conditions for a low-salinity Enhanced Oil Recovery (EOR) effect in carbonate oil reservoirs. *Energy Fuels* **2012**, *26* (1), 569–575.
- (33) Masalmeh, S.; Al-Hammadi, M.; Farzaneh, A.; Sohrabi, M. *Low salinity water flooding in carbonate: Screening, laboratory quantification and field implementation*, Society of Petroleum Engineers - Abu Dhabi International Petroleum Exhibition and Conference 2019, 2019 DOI: 10.2118/197314-MS.
- (34) Kakati, A.; Kumar, G.; Sangwai, J. S. Low Salinity Polymer Flooding: Effect on Polymer Rheology, Injectivity, Retention, and Oil Recovery Efficiency. *Energy Fuels* **2020**, *34* (5), 5715–5732.
- (35) Al-Ibadi, H.; Stephen, K.; MacKay, E. *Heterogeneity Effects on Low Salinity Water Flooding*, Society of Petroleum Engineers - SPE Europec Featured at 82nd EAGE Conference and Exhibition, 2020 DOI: 10.2118/200547-MS.